Originally published as:

Košler, J., Jackson, S. E., Yang, Z., Wirth, R. (2014): Effect of oxygen in sample carrier gas on laser-induced elemental fractionation in U–Th–Pb zircon dating by laser ablation ICP-MS. - *Journal of Analytical Atomic Spectrometry*, *29*, p. 832-840

DOI: http://doi.org/10.1039/c3ja50386k

JAAS

PAPER

View Article Online
View Journal | View Issue

Published on 18 February 2014. Downloaded by GFZ POTSDAM WISSENSCHAFTSPARK on 29/10/2014 10:14:04.

Cite this: *J. Anal. At. Spectrom.*, 2014, **29**, 832

Effect of oxygen in sample carrier gas on laser-induced elemental fractionation in U–Th–Pb zircon dating by laser ablation ICP-MS

Jan Košler,*[abc] Simon E. Jackson,[b] Zhaoping Yang[b] and Richard Wirth[d]

Received 11th December 2013
Accepted 18th February 2014

DOI: 10.1039/c3ja50386k

www.rsc.org/jaas

Thermal breakdown of zircon during laser ablation sampling for ICP-MS analysis results in decoupling of Si from Zr, and Pb from U + Th, following the reaction $ZrSiO_4$(U, Th, Pb) = ZrO_2(U, Th) + SiO_2(Pb). The rate of the laser-induced elemental fractionation can be linked to the concentration of oxygen in the ambient He sample carrier gas. Deposition of ZrO_2 and SiO_2 on the walls of the ablation craters is enhanced by the presence of oxygen during ablation, and the composition of the deposit is dominated by ZrO_2. This study shows that even a small amount of oxygen (*e.g.*, 500 ppm) added to the sample carrier gas can shift the U–Pb ages of zircon by as much as 9%, which is well beyond the typical analytical uncertainty of LA-ICP-MS zircon dating. Addition of up to 2000 ppm oxygen to the sample carrier also increases the instrument sensitivity by as much as 3 times for light elements and *ca.* 1.5 times for heavy elements. The increase in sensitivity is accompanied by an increase in the U and Th oxide formation, suggesting that the signal enhancement is not related to the concomitant M^+ and MO^+ ion formation, but rather to the improved atomization and ionization capabilities of the mixed gas ICP. The study shows that maintaining a constant level of O_2 throughout the ablation cell over an analytical session at the time of analysis is a prerequisite for further improvements in the repeatability of U–Pb LA ICP-MS dating of zircon.

Introduction

Since the first attempts to date accessory minerals by U–Th–Pb laser ablation ICP-MS (LA-ICP-MS) some twenty years ago,[1–4] this technique has become increasingly popular in the geological community. The mineral zircon (tetragonal form of $ZrSiO_4$) is the most commonly studied accessory phase in magmatic, metamorphic and sedimentary rocks[5] because of its widespread abundance, resistance to abrasion and dissolution in natural environments, its ability to quantitatively retain trace elements over geological time and its low initial content of non-radiogenic Pb.

Determination of U, Th and Pb isotopes in zircon by LA-ICP-MS is complicated due to the effects of laser-induced elemental fractionation of Pb relative to U and Th, which are affected by variations in the zircon matrix (chemistry, radiation damage, crystallinity and colour), and mass discrimination of isotopes in ICP-MS. The potential errors in age determination due to these processes can be reduced or eliminated by matrix-matched calibration and a series of mathematical corrections. The uncertainty associated with the correction for laser-induced elemental fractionation typically dominates the uncertainty budget of U–Th–Pb dating by LA-ICP-MS and an inaccurate correction will result in an erroneous age.

It has been demonstrated that the phase separation and formation of particles of variable size and composition are the primary causes of laser-induced elemental fractionation,[6] and that the element decoupling can be further enhanced by variable aerosol transport and processes in the ICP.[7] Interaction of laser radiation with zircon typically results in thermal breakdown of $ZrSiO_4$ to ZrO_2 and SiO_2 and formation of aerosol particles with different compositions, sizes and transport properties.[8] As a result of the preferential partitioning of U + Th and Pb into ZrO_2 and SiO_2 phases, respectively, the decomposition of zircon by transfer of laser heat can efficiently fractionate these geochronologically important trace elements, potentially resulting in erroneous U–Th–Pb ages obtained by LA-ICP-MS dating.

Previous studies have linked the degree of laser-induced decoupling of U + Th from Pb in zircon in any analysis to the chemical composition of the zircon matrix[9] and the amount of radiation damage accumulated since the last annealing of zircon.[10] More recently the obtained laser ablation ICP-MS data for a suite of well characterized zircon samples with a range of compositions and accumulated radiation damage[11] suggest that these factors alone cannot explain the observed variations in the

[a]*Department of Earth Science, University of Bergen, Allegaten 41, Bergen, N-5007, Norway. E-mail: jan.kosler@geo.uib.no*

[b]*Geological Survey of Canada, Natural Resources Canada, 601 Booth St., Ottawa, Ontario, K1A 0E8, Canada*

[c]*Czech Geological Survey, Klárov 3, Prague 1, CZ-118 21, Czech Republic*

[d]*Helmholtz Centre Potsdam, GFZ German Research Centre for Geosciences, 3.3 Telegrafenberg, 14473 Potsdam, Germany*

This journal is © The Royal Society of Chemistry 2014

Published on 18 February 2014. Downloaded by GFZ POTSDAM WISSENSCHAFTSPARK on 29/10/2014 10:14:04.

rate of laser-induced elemental fractionation; they may, however, affect the kinetics of the phase separation during the thermal breakdown of zircon.

In this study, we explore the effects of oxygen present in the sample carrier gas on the laser-induced elemental fractionation of Pb and U + Th during LA-ICP-MS analysis of zircon. As a major component of air, oxygen is a ubiquitous contaminant of the He carrier gas used in LA-ICP-MS to transport the ablated material from the sample cell to the ICP. In addition to its potential low-level presence as a natural contaminant in the He supply, its most insidious sources are diffusion through, and degassing of, supply tubing and desorption from surfaces. Monitoring of gas background signal intensities for atmospheric gases or polyatomic ions of atmospheric gases (*e.g.*, masses 29 or 56) shows that this can be significant for several hours after starting up the instrumentation. If oxygen plays a significant role in controlling the degree of laser-induced Pb–U + Th fractionation, better control of its effects would lead to improved accuracy of U–Th–Pb dating by LA-ICP-MS.

Laser-induced elemental fractionation of Pb and U + Th in zircon

Laser-induced elemental fractionation in ICP-MS refers to the change of measured signal intensity ratios on the time scale of a single analysis, typically several hundreds to thousands laser pulses, or between analyses. It has been demonstrated that the thermal effects of laser radiation are efficient in triggering the breakdown of tetragonal $ZrSiO_4$ to a mixture of tetragonal, monoclinic and amorphous ZrO_2 and a mixture of amorphous and high-temperature SiO_2 phases[8] at *ca.* 1680 °C.[12] The corresponding thermally induced reactions were previously described from zircon heating laboratory experiments[13,14] and natural rocks that underwent a high-temperature event.[15] It has also been shown that the thermal breakdown of zircon is not limited to nano-second laser ablation but has also been observed during femto-second laser ablation of zircon.[16] The crystal lattice parameters of the newly formed ZrO_2 and SiO_2 phases are suitable for incorporation of U + Th and Pb, respectively, effectively decoupling the radiogenic Pb produced in zircon from its parent elements. The newly formed ZrO_2 and SiO_2 phases form particles with different size distributions[8] that may be transported to the ICP with different efficiencies and, or, may atomise and ionise at different depths within the ICP, resulting in the observed U + Th and Pb fractionation.

The rate of elemental fractionation during laser ablation of zircon is related to the progress of the zircon decomposition reaction and is proportional to the inner surface area of the ablation crater, and hence to the crater aspect ratio.[17,18] The rate of laser-induced elemental fractionation is significantly reduced for shallow craters with a low aspect ratio during static ablation or when using dynamic ablation (laser raster or line scan).[19,20] In addition, femtosecond laser ablation[21,22] and ablation with a short (DUV) laser wavelength[23] were reported to have reduced laser-induced elemental fractionation. The methods used to correct for laser-induced elemental fractionation include calibration relative to an external zircon standard, mathematical corrections of the fractionating signal or a combination of these two techniques. Corrections made by comparison to an external zircon standard are limited by the need to use the same ablation conditions and corresponding ablation intervals for the unknown and reference samples. This type of correction is prone to error caused by differences in the ablation rates between the unknown and reference zircons due to their chemically and structurally different matrices. The mathematical corrections relate the fractionation rate to the crater diameter[24] or extrapolate the fractionation trend to the start of the ablation process. The extrapolation can be done independently for each unknown and reference zircon[25] or it can be modeled for the reference zircons and then applied to the unknown samples.[26,27] Jackson[28] and later also Kuhn *et al.*[29] proposed an alternative correction method that makes use of the empirically observed correlation between elemental ratios of Si/Zr and Pb/U.

When U–Pb and Th–Pb zircon analyses are to be combined, an additional pre-requisite is that U and Th should not be decoupled during the ablation, transport and ionization in the ICP source of the mass spectrometer. The two elements are typically accommodated in the ZrO_2-rich aerosol particles but due to the incomplete atomization of refractory phases (oxide forming species) in the ICP, and because of the temporal variation of the mean particle size during the course of a laser ablation analysis, the U/Th signal ratio can show a significant variation over the time span of a single analysis.[30,7] This ICP-induced elemental fractionation can be partly compensated for by particle filtering,[7] by using a femtosecond pulse width[22] and by ablating with a shorter (deep UV) wavelength of the laser.[23] Alternatively, sampling a different part of the ICP can also compensate for the ICP-induced elemental fractionation. This can be achieved by changing the plasma RF power, distance between the ICP and the interface or ICP gas flows.

Effects of molecular gasses in LA-ICP-MS

The composition of the ambient gas during laser ablation sampling (often referred to as sample carrier gas) can have a significant effect on the results of LA-ICP-MS analysis. In the ablation cell, it impacts the formation and transport of the ablated aerosol. Downstream from the ablation cell, the sample carrier gas enters the ICP and its composition plays an important role in the atomization and ionization of the sample. The presence of foreign (often molecular) gasses in the sample carrier gas originates from gas impurities, degassing of inner surfaces of the ablation cell and tubing, diffusion of air through the tubing walls, any leaks and ablation of samples that produce gaseous species. In a typical LA-ICP-MS experiment, it is often difficult to separate the effects of the sample carrier gas during processes that occur at the ablation site and in the ICP but it is practical to discuss the two effects separately.

Composition effect of sample carrier gas on the ablation and transport of aerosol

The early laser ablation ICP-MS studies used Ar as the sample carrier gas, presumably because it did not require different

Published on 18 February 2014. Downloaded by GFZ POTSDAM WISSENSCHAFTSPARK on 29/10/2014 10:14:04.

settings of the ICP matching network that was tuned for the Ar plasmas and because the superior transport properties of He were not yet recognized. For routine analysis, use of Ar as the sample carrier gas was later replaced by He[17,31] because its higher thermal conductivity and lower density and viscosity improve sample removal, reduce plasma shielding and result in better overall transport efficiency during ablation at atmospheric pressure. Avoiding the use of Ar as the sample carrier gas also reduces the formation of Ar-based species that in some types of analysis may interfere with the analytes.[32]

In an attempt to control the elemental fractionation of Pb and U, Hirata[33] introduced freon R-134a gas (1,1,1,2-tetrafluoroethane) into the He sample carrier gas to the ablation cell. The freon reacted with U to produce a volatile U fluoride compound (UF_6) under high temperature conditions at the ablation site, which improved the transmission efficiency for U. In another study, addition of oxygen to the He carrier gas was shown to have a significant effect on elemental fractionation during the ablation of silicate and sulphide samples.[34] Concentrations of O_2 in the He sample carrier gas as low as few hundred ppm were sufficient to affect the aerosol properties (possibly due to redox reactions in the plasma plume) and to change the extent of elemental fractionation. An application where this applies is LA-ICP-MS analysis of samples that will not fit in the ablation cell, where ablation in an open transport system is typically used. Sampling is carried out in air,[35,36] which is then exchanged for Ar in a gas converter apparatus and introduced into ICP-MS instruments. The analytical performance of the open transport setup is comparable to a standard closed transport LA-ICP-MS.[36]

Effect of gas composition on the atomization and ionization in the ICP

The effect of ICP gas composition on the analytical performance of the ICP-MS has been a subject of numerous studies (see the overviews in ref. 37–40). Most of them explored the addition of polyatomic gasses such as nitrogen, hydrogen, oxygen, methane and air, or monoatomic gasses (helium or xenon) to Ar with the aim of improving the atomization and ionization power of the ICP. The foreign gasses were added to all three gas streams of the ICP, often with notable effects on the signal intensity. However, these experiments could often not be reproduced by different instruments in other labs. Enhancement of the signal intensity by addition of nitrogen to the ICP has been explained by better thermal conductivity of N_2 compared to Ar,[41,42] which should facilitate the transfer of energy between the gas and sample aerosol within the plasma (thermal conductivity of N_2 at 7000 K is 32× higher compared to Ar[43]). Addition of N_2 to the Ar ICP also reduces molecular interference of MO^+, since the formation of strong bonds in the NO molecules effectively scavenges O^+ ions present in the ICP.[41,43] Similar to N_2, the effect of signal enhancement due to improved thermal conductivity was reported for the addition of H_2.[40] In another study, signal enhancement was observed as a result of addition of O_2 to the ICP for the purpose of oxidising carbon during the analysis of organic compounds, and also to limit the deposition of reduced organic material on the sampling cone.[44]

The lack of reproducibility of experiments with mixed-gas plasmas, and especially contradicting results for signal enhancement by addition of molecular gases to the Ar ICP have led to limited application of this technique. Difficulties in achieving signal enhancement by the addition of foreign gasses to the ICP by some laboratories have been attributed to air entrainment into the ICP[45] that is, when at atmospheric pressure, effectively a mixed-gas plasma (Longerich, pers. com. 2013). Subject to the variable amount of air that is already present in the Ar, the introduction of additional gas may or may not improve the atomization and ionization power of the ICP.

Experimental setup

The instrumental setup used for the laser ablation experiments is shown in Fig. 1. We used a 193 nm ATL excimer laser that was part of an Analyte 193 (Photon Machines Inc.) laser ablation system at the Geological Survey of Canada to ablate the GJ-1 and Mud Tank zircon samples.[46,47] The laser was fired at a repetition rate of 10 Hz and energy density of 6.4 J cm^{-2} to produce single, 26 μm wide craters in zircon sample GJ-1. The two-volume HelEx sample cell was flushed with a mixture of He and O_2 gases (total 1 l min^{-1}) *via* the gas inlet into the base of the cell. Variable nominal concentrations of oxygen (0–2000 volume ppm) in the He sample carrier gas were achieved by mixing, upstream from the ablation cell, pure He (better than 99.999%) with a mixture of He + O_2 (500 ppm) or with pure oxygen to achieve higher O_2 contents (up to 2000 ppm). The gas flows were controlled using external MKS (model 1479A/246C) and Alicat Scientific (MC series, part of the Analyte 193 laser ablation system) mass flow controllers. The sample carrier gas containing the ablated aerosol was then mixed with Ar (0.9 l min^{-1}) in a T-junction (without any signal smoothing device) and introduced into the shielded ICP (RF = 1200 W) of a quadrupole ICP-MS (Agilent 7700x). Signal intensities of ^{29}Si, ^{96}Zr, $^{206,207,208}Pb$, ^{232}Th, ^{238}U, ^{248}ThO and ^{254}UO were measured in time-resolved mode with respective dwell times of 5, 5, 15, 50, 10, 10 and 10 ms. A typical analysis consisted of data acquisition of a gas blank (30 s) followed by a 60 s acquisition of laser ablation signal (600 laser pulses).

Data were processed off-line in an MS Excel spreadsheet. The data reduction included correction for gas blank and

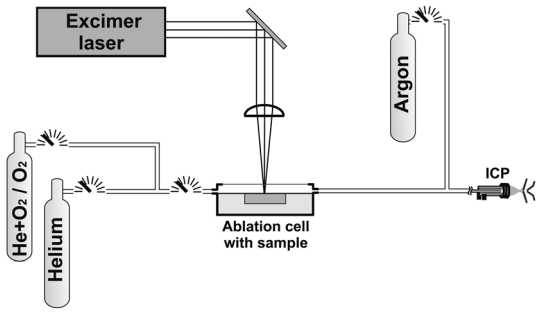

Fig. 1 Experimental setup for laser ablation sampling of zircon at variable oxygen concentrations in the He sample carrier gas.

 This journal is © The Royal Society of Chemistry 2014

Published on 18 February 2014. Downloaded by GFZ POTSDAM WISSENSCHAFTSPARK on 29/10/2014 10:14:04.

calculation of the slope and intercept values for the observed fractionation trends.[48] In addition to the mean values of the signal intensity ratios, the slope and the intercept (value of the signal intensity ratio at the start of ablation) were used to characterize the laser-induced elemental fractionation. These were calculated assuming a linear change of the signal intensity ratios with the ablation time (*i.e.*, the number of laser pulses applied to the sample). Prior to the calculation, all time-resolved signal intensity ratios were visually inspected for linearity and lack of excursions that could impact on the calculated results.

In the second part of the study, we used identical experimental parameters, except for firing 1500 laser pulses using a beam diameter of 86 μm, to ablate and analyze the Mud Tank zircon sample at variable O_2 concentrations in the He sample carrier gas. The Mud Tank zircon, rather than the GJ-1 zircon, was used for this part of the study because it was available to us in greater quantities and larger pieces. The zircon sample was sectioned using a low speed saw and the two perpendicular-cut surfaces of each part of the sample were polished before the zircon grain was re-assembled in the sample holder of the HelEx ablation cell. This formed a flat polished sample surface that was perpendicular (*i.e.*, horizontal) to the incident laser beam with a joint between the two parts of the sample that was parallel to the laser beam (*i.e.*, vertical). This sample arrangement allowed the Mud Tank zircon to be ablated down the joint and, following the ablation, the two parts of the sample to be separated, exposing the cross-section of the ablation pits (Fig. 2).

The laser pits in one part of the Mud Tank zircon sample were filled with epoxy to form a flat surface that was coated with a protective layer of Pt. The wall and bottom parts of the pits were sectioned by a focused ion beam (FIB) that uses an accelerated beam of Ga ions to sputter the material from the target and produces electron-transparent foils (*ca.* 20 × 10 × 0.12 μm) for the subsequent TEM study [(ref. 49 and 50), Fig. 2]. The TEM analytical work was carried out at GFZ Potsdam using an FEI Tecnai G2 F20 X-Twin system using a 200 kV electron beam generated from a field emission gun. The TEM study included bright-field and dark-field imaging, high-angle annular dark field (HAADF) and high-resolution transmission electron microscopy (HRTEM) imaging as well as electron diffraction analysis (fast Fourier transform – FFT) and energy dispersive X-ray analysis (EDX). The spatial resolution of the EDX is controlled by the beam diameter, which was *ca.* 1–2 nm.

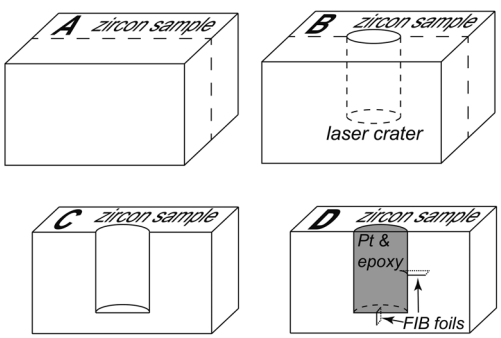

Fig. 2 Schematics of sample preparation for the FIB/TEM study. (A) Sectioning the zircon grain, (B) laser ablation along the joint, (C) separation of the two parts of the sample, (D) sampling the wall and the bottom of the ablation pit by a focused ion beam (the laser pit was filled with epoxy and coated with the protective Pt layer).

Results

Effect of oxygen addition on measured signal intensity

Mean signal intensities obtained by LA-ICP-MS analysis of the GJ-1 zircon at different levels of oxygen in the He sample carrier gas are shown in Fig. 3. The data were collected on two different days and using two different experimental setups. During day 1, the oxygen dilution was achieved by the addition of the He + O_2 mixture to the stream of pure He *via* a mass flow controller. This arrangement was used to achieve low oxygen concentrations (up to 500 ppm). To achieve higher oxygen concentrations (500 to 2000 ppm) for the experiments run on day 2, the He + O_2 mixture was replaced by a pure oxygen supply. The data suggest that the instrument sensitivity was somewhat (*ca.* 30%) lower during the experiment done on day 2 but data from both days show a similar trend. As expected, the addition of oxygen to the He sample carrier gas increased the abundance of oxide ions in the ICP. In this case, an increase from 30 to 14 000 cps and from 450 to 120 000 cps was observed for $^{232}ThO^+$ and $^{238}UO^+$, respectively when the oxygen level increased from 0 to 2000 ppm. At the same time, a signal intensity increase was observed for masses ^{29}Si (2.03 to 6.06 million cps), ^{96}Zr (42.4 to 84.7 million cps), ^{206}Pb (3750 to 6500 cps), ^{232}Th (29 000 to 42 000 cps) and ^{238}U (600 000 to 916 000 cps). Correspondingly, the oxide formation ($MO^+/M^+ \times 100$) increased from 0.1 to 33% and from 0.08 to 13% for $^{232}ThO^+$ and $^{238}UO^+$, respectively (Fig. 3D). Overall, while the increase in oxide ion abundance with increasing oxygen concentration in the He sample carrier gas was *ca.* 270–470 fold, the increase in signal intensity for the measured elemental ions varied between 3 and 1.5 fold for the light and heavy elements, respectively, effectively shifting the maximum of the instrument's mass response curve towards lighter masses. The signal intensities of $^{232}ThO^+$ and $^{238}UO^+$ show a linear increase with increasing concentration of oxygen in the He sample carrier gas up to *ca.* 500–1000 ppm O_2, and it is not accompanied by a complementary decrease of the signal of elemental ions as it would be the case if there was a competition between concomitantly produced MO^+ and M^+ ions.

Effect of oxygen addition on laser-induced elemental fractionation

The effects of oxygen addition to the He sample carrier gas on laser-induced fractionation of elements are shown in Fig. 4. The mean values of the Si/Zr and Pb/U ratios determined from the ablation of the GJ-1 zircon increase by *ca.* 9% between 0 and 500 ppm of added oxygen. The 9% increase of $^{206}Pb/^{238}U$ can be translated to an age difference of ~60 million years for this sample. The initial rapid increase is followed by a slower rise of the ratios up to 2000 ppm of added oxygen. In gross terms, the trends of increase in mean values of Si/Zr and Pb/U ratios with increasing amount of added O_2 follow each other. A closer

Published on 18 February 2014. Downloaded by GFZ POTSDAM WISSENSCHAFTSPARK on 29/10/2014 10:14:04.

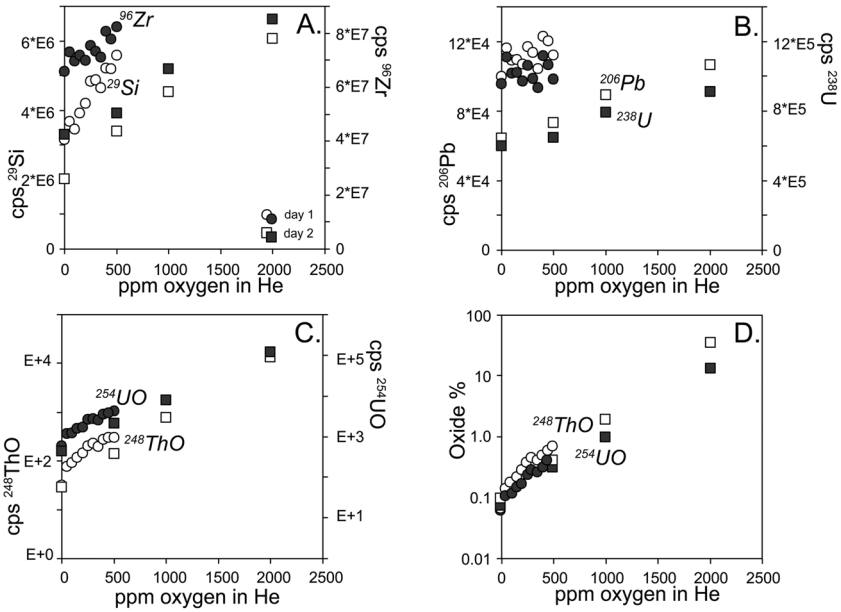

Fig. 3 The effects of oxygen in the He sample carrier gas on the measured signal intensities of (A) ^{29}Si and ^{96}Zr, (B) ^{206}Pb and ^{238}U and (C) ^{248}ThO and ^{254}UO. The proportion of ^{248}ThO and ^{254}UO calculated to be $MO^+/M^+ \times 100$ [%] is shown in (D).

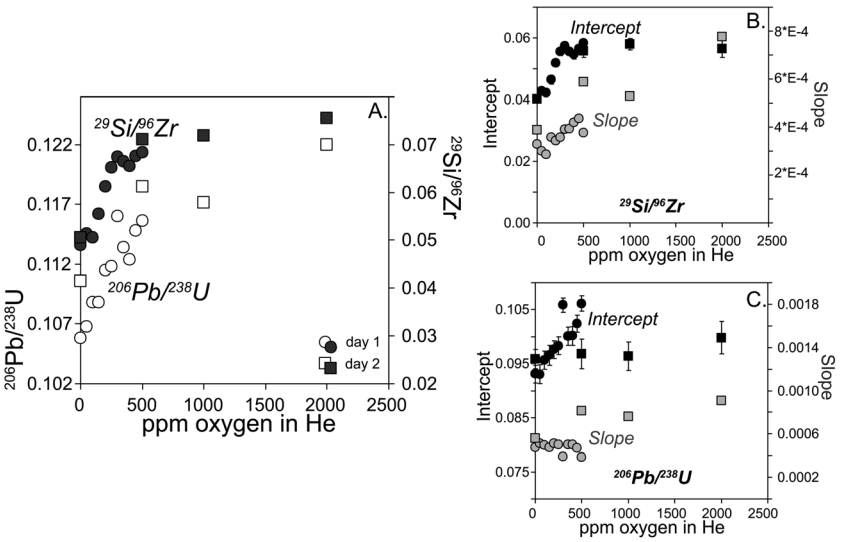

Fig. 4 The effects of oxygen in the He sample carrier gas on (A) the measured signal intensity ratios of ^{29}Si/^{96}Zr and ^{206}Pb/^{238}U. Diagrams (B) and (C) show the separate effects of the oxygen concentration in the He sample carrier gas on the slope and the intercept[48] of the elemental fractionation trends of ^{29}Si/^{96}Zr and ^{206}Pb/^{238}U, respectively. Uncertainties on the intercept values are 1 sigma.

inspection of the fractionation trends shows that in the case of the Si/Zr signal intensity ratios, the change of the mean ratio value with increasing concentration of O_2 is due to the increase of both the slope and the intercept values of the Si–Zr fractionation trend. However, in the case of the Pb/U signal intensity ratios, the change of the mean value can be attributed mainly to the change of the intercept value, while the slope of the fractionation trend remains virtually the same for oxygen concentrations in the He sample carrier gas between 0 and 500 ppm. Since it is usually the mean value of the Pb–U fractionation trend or the value of its intercept (the value of the Pb–U ratio at the start of laser ablation) that are used to calculate the U–Pb ages in laser ablation ICP-MS dating of zircon, either of these two approaches might result in erroneous U–Pb zircon ages when the oxygen concentration in the ablation cell varies between analysis of samples and standards (*e.g.*, during the period of significant degassing of tubing, samples and ablation cell surfaces after instrument start up).

Oxygen-induced phase changes during laser ablation of zircon

Secondary electron imaging of the ablation pits produced in the Mud Tank zircon sample at different concentrations of oxygen in the He sample carrier gas shows layers of the molten or

 This journal is © The Royal Society of Chemistry 2014

Published on 18 February 2014. Downloaded by GFZ POTSDAM WISSENSCHAFTSPARK on 29/10/2014 10:14:04.

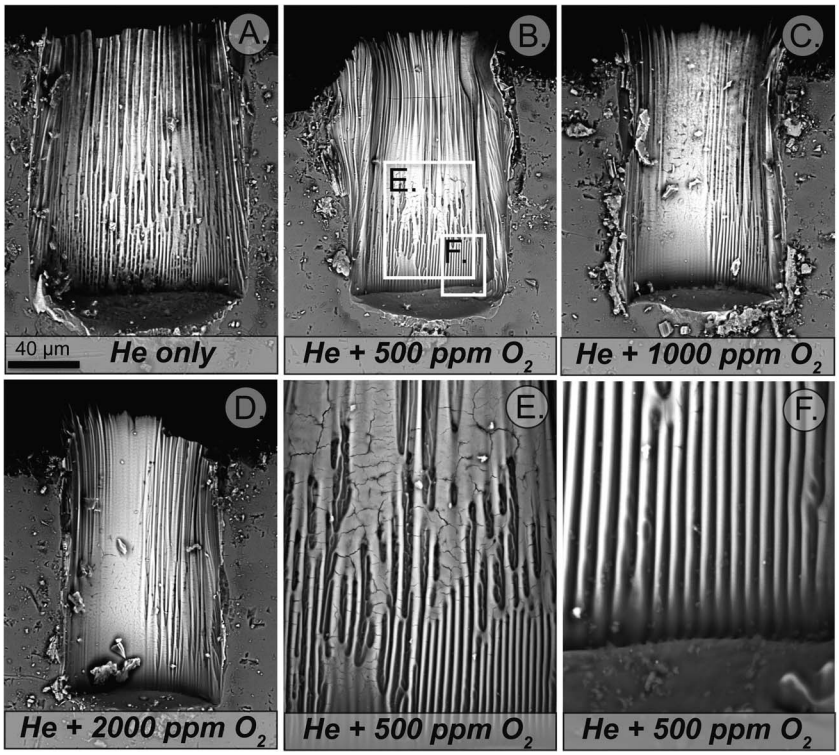

Fig. 5 Secondary electron images of the ablation pits produced in the Mud Tank zircon sample at different concentrations of oxygen in the He sample carrier gas. Figures (E) and (F) show details of the wall deposit with cooling cracks and corrugated surfaces.

microcrystalline material deposited on the ablation pit walls, as well as some melt at the bottom of the pits (Fig. 5). The layer deposited on the walls shows corrugated, vertically oriented structures with later cooling cracks that cut across the corrugations. With an increasing amount of oxygen in the He carrier gas, the wall deposits show a change from a discontinuous and intensely corrugated deposit at low oxygen concentrations to a smooth, continuous and more voluminous layer at higher oxygen concentrations. In contrast to the crater walls, the deposits at the bottom of the pits are smooth, featureless and thinner compared to the deposit on the walls. No visible variation in the structure and composition of the pit bottoms has been observed for different concentrations of oxygen in the He sample carrier gas.

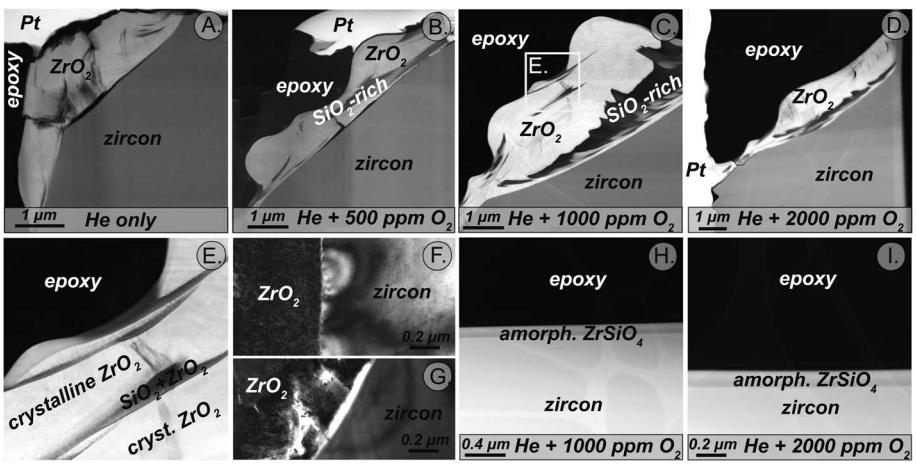

Fig. 6 Transmission electron microscopy images of the FIB foil cut from the laser ablation craters in the Mud Tank zircon produced at different concentrations of oxygen in the He sample carrier gas. (A–D) High-angle annular dark field (HAADF) images of the FIB foils from the crater walls, and (E) details of the wall structure in (C). (F and G) Bright field (BF) images of the interface between the crater walls and the wall deposits produced with pure He sample carrier gas, (H and I) HAADF images from the bottoms of the laser craters. Since the structure and composition of the bottom part of the craters do not change with the oxygen concentration, only two images are shown.

Published on 18 February 2014. Downloaded by GFZ POTSDAM WISSENSCHAFTSPARK on 29/10/2014 10:14:04.

High-angle annular dark field (HAADF) images and bright (BF) and dark (DF) field images obtained by TEM from the focused ion beam (FIB) foil cut from the wall and the bottom of the pits ablated in the Mud Tank zircon at different concentrations of oxygen in the He sample carrier gas are shown in Fig. 6. The HAADF images suggest that the deposit on the crater walls is mainly made of coarsely crystalline monoclinic ZrO_2, nanocrystalline ZrO_2 and amorphous SiO_2. Only a small proportion of the wall deposit is composed of tetragonal $ZrSiO_4$. The interface between zircon that forms the crater wall and the mixture of ZrO_2 and SiO_2 phases in the layer is sharp (*cf.* the BF and DF images in Fig. 6), suggesting that the phases that constitute the wall layer formed prior to being deposited on the crater walls; *i.e.*, that the ZrO_2 and SiO_2 phases did not form *in situ*. The deposit is heterogeneous on the micron and submicron scale, with discrete domains formed by different phases. The texture of the layer resembles that of a flowing viscous liquid, suggesting that the material was plastic and perhaps partly molten when the layer formed, and, although its thickness varies within the individual craters, it generally increases with increasing concentrations of oxygen in the He sample carrier gas. In contrast to the deposit on the crater walls, the phase composition revealed by the FIB foil cut from the bottom of the craters is more uniform. A 150–180 nm thick layer of glass, which has a stoichiometric composition of $ZrSiO_4$, covers the bottoms of all the craters. The thickness of the glass layer does not vary with changing concentrations of oxygen in the He sample carrier gas.

Discussion

Phase separation during the thermally induced breakdown of zircon

The phase change of $ZrSiO_4$ to ZrO_2 and SiO_2 observed in this study as a result of interactions of DUV excimer laser radiation with natural zircon is similar to the laser-induced thermal effects observed by Kosler *et al.*[8] for zircon ablated by a solid state ns UV Nd:YAG laser ($\lambda = 266$ nm), by Wang *et al.*[51] for IR CO_2 laser ablation and also for UV femtosecond laser ablation of zircon (ref. 16 and the unpublished FIB/TEM data of Kosler and Wirth for zircon ablated by a UV femtosecond laser). The previously published TEM analysis of ablation craters produced by the UV Nd:YAG laser with a poor energy beam profile[8] is indicative of an *in situ* phase reaction in the crater walls. By contrast, the present study of craters produced with the DUV excimer laser with a significantly better beam energy profile shows a sharp interface between the crater walls ($ZrSiO_4$) and the wall deposit (ZrO_2 + SiO_2 + $ZrSiO_4$), suggesting that the phase reaction took place prior to the deposition. There is also a notable difference between the structure of the crater walls and their bottoms. The surfaces of the crater bottoms are clean with just a thin layer (150–180 nm) of $ZrSiO_4$ glass while the deposits on the walls contain up to several μm thick layers of coarsely crystalline monoclinic and nanocrystalline ZrO_2 (dominant phase), amorphous SiO_2 and small amounts of tetragonal $ZrSiO_4$. This observation points to the phase reaction $ZrSiO_4 = ZrO_2 + SiO_2$ taking place during or after the removal of material from the crater bottom, but prior to, or at the time of, its deposition on the crater wall. It also suggests that the composition of aerosol produced by laser ablation of zircon is already fractionated when it leaves the ablation crater. It should also be noted that formation of $ZrSiO_4$ melt at the bottom of laser craters would not be expected because zircon melts incongruently or decomposes to ZrO_2 and SiO_2 prior to melting,[52] and the amorphous state of the melt is not stable during cooling.[53] The thin layer of $ZrSiO_4$ glass is likely to be non-stable and its existence can only be explained by fast quenching between the laser pulses.

The banded structure of the wall deposits, where the SiO_2-rich layers alternate with the more voluminous ZrO_2-rich layers (*cf.* Fig. 6), may form during the deposition as a result of sputtering and re-deposition of the material on the crater walls in combination with small variations in the ablation parameters or after the deposition of the layer by phase separation within the hot and presumably plastic wall deposit. The apparent volume dominance of the ZrO_2 phases over the SiO_2 phases in the wall deposit is consistent with the higher condensation temperature of ZrO_2 (4300 °C) compared to SiO_2 (2230 °C) and its preferential condensation closer to the ablation site, and with the observed increase of Si/Zr and also Pb/U ratios during the ablation (positive slopes of the Si–Zr and Pb–U fractionation trends in Fig. 4B and C, respectively). The function of the crater walls as efficient scavengers of the ablated aerosol has been pointed out by previous studies[17,18] and it is reflected in the commonly used laser ablation sampling strategies that typically aim at the crater aspect (depth/diameter) ratio of less than 1 (ref. 20) in order to reduce the laser-induced elemental fractionation. The present study, for the first time, provides data that illustrate in detail the mechanisms of elemental fractionation within the ablation craters, namely the importance of the crater walls during laser ablation of zircon.

The element fractionation trends for different concentrations of oxygen in the He sample carrier gas shown in Fig. 4 suggest that the Si–Zr fractionation follows only partly the fractionation of Pb–U, despite the respective compatibilities of Pb and U with the SiO_2 and ZrO_2 phases. This is best shown by a comparison of the intercept and slope values for the $^{29}Si/^{96}Zr$ and $^{206}Pb/^{238}U$ fractionation trends at different concentrations of oxygen (*cf.* Fig. 4). Both the slope (which reflects the fractionation rate) and the intercept (which reflects the mass bias) of the $^{29}Si/^{96}Zr$ fractionation trend change with increasing concentration of oxygen, while for the $^{206}Pb/^{238}U$ fractionation, the slope remains virtually constant. It has been proposed[28,29] that the Si/Zr values may be used to correct for the Pb/U laser-induced elemental fractionation during laser ablation of zircon. The results of this experiment suggest that such a correction will only work, provided that there is no ambient oxygen available during laser ablation or when the oxygen concentration remains constant during the analysis. Some of the data in Fig. 4 show a shift in the Pb/U intercept values between measurements that were done on two different days, as well as the change in the increase of the value of the intercept with the added O_2 to the He sample carrier gas at *ca.* 500 ppm O_2. These changes are interpreted as resulting from the variable mass bias between the two days and at high concentrations of O_2 in the ICP.

 This journal is © The Royal Society of Chemistry 2014

Published on 18 February 2014. Downloaded by GFZ POTSDAM WISSENSCHAFTSPARK on 29/10/2014 10:14:04.

Sources of oxygen and its effects on laser-induced elemental fractionation

Both our SEM and TEM observations suggest that the thickness of the wall layers composed of a mixture of monoclinic and nanocrystalline ZrO_2, amorphous SiO_2 and some tetragonal $ZrSiO_4$ increases with increasing ambient concentrations of O_2, which, in turn, positively correlates with the Si–Zr and Pb–U fractionation patterns (*cf.* Fig. 4–6). This leads to the conclusion that the concentration of oxygen in the ablation cell is an important factor that controls the laser-induced elemental fractionation during laser ablation of zircon.

The amount of oxygen that is needed to significantly change the element fractionation rates is fairly small. Our experiment suggests that only 500 ppm O_2 in the ablation cell can change the apparent U–Pb age of zircon by as much as 9% which makes the analysis useless for many geological applications. Such low concentrations are easily achievable through impurities in the sample carrier gas, degassing of the inner surfaces of tubing, samples and ablation cell, residual air and moisture present in the ablation cell after it was opened to the atmosphere and potential leaks in the system. The mere presence of oxygen in the ablation cell would not be an obstacle to an accurate analysis, provided that it is constant with the time and the location within the cell so that corresponding data can be obtained from samples and standards. Spatial and temporal variations in the oxygen concentration in the ablation cell can, however, result in erroneous U–Pb ages obtained by laser ablation ICP-MS analysis of zircon.

Another potential source of oxygen is the sample itself. Laser ablation of oxides and silicates, such as zircon, will break the atomic bonds in the structure and release oxygen to the sample carrier gas. It has been estimated[34] that a typical ablation crater in silicate glass (60 μm wide and 100 μm deep laser pit in NIST 612) can produce up to 0.6 μg of oxygen. If some of this is present as free oxygen, high concentrations of oxygen may be present at the ablation site, which may significantly alter the elemental fractionation pattern. The amount of oxygen released by ablation of zircon from a crater that is 26 μm in diameter and 60 μm deep (such as the ablation craters produced in zircon GJ-1 in this study) is 0.05 μg, which represents a quantity that could significantly affect the laser-induced Pb–U and Pb–Th elemental fractionation, particularly if there is a progressive increase in the oxygen concentration in the pit as it deepens by ablation. Accordingly, it is important that the matrices of samples and standards are identical (or at least very similar) in their composition and oxygen content. This may be difficult to achieve for natural samples that typically have a range of compositions and are rarely homogeneous. In the case of the mineral zircon, an additional complexity comes from its variable ages and U (Th) contents that lead to a variable degree of radiation damage (metamictization). Allen and Campbell[10] and Kooijman *et al.*[11] have recently reported on the effects of radiation damage in zircon on the accuracy of U–Pb zircon ages obtained by laser ablation ICP-MS. While the former study concluded that the effects were systematic (there was a correlation between the calculated radiation damage and bias of the U–Pb age), the data presented in the latter study show no such correlation. Given that metamictization of zircon by radiation damage typically leads to an increase of oxygen content in its structure,[54] laser ablation of zircons with a variable degree of radiation damage can liberate different amounts of oxygen that can affect the elemental fractionation patterns to a different degree. The relationship between radiation damage, variable amount of oxygen that is prone to liberation during the ablation of variably metamict zircons and the fractionation pattern of Pb–U (and also Si–Zr) may explain the apparent discrepancy in conclusions of the two aforementioned studies.[10,11]

Oxygen effects on ICP-MS signal enhancement

The observed enhancement of instrument sensitivity by as much as 3 times due to addition of small amount of oxygen to the He sample carrier gas was accompanied by an increase in oxide signal intensity by as much as 470 times. This would not be the case if there was competition between the M^+ and MO^+ ion formation; the observation rather suggests that addition of small amount of oxygen to the ICP can improve its atomization and ionization capabilities. The likely reason for this sensitivity enhancement is, similar to the addition of other molecular gasses, such as N_2 or H_2, which improves the heat transfer between the gas and sample aerosol. This is in accord with the computer simulations of the addition of O_2 to the nebulizer gas reported by Cai *et al.*[55] that resulted in an increase of the plasma temperature.

Concluding remarks

The experimental data from this study show that even a small amount of oxygen present in the ambient gas during the ablation of zircon can have pronounced effects on the elemental fractionation of Si–Zr and Pb–U. This points to the importance of maintaining constant and preferably low levels of ICP gas impurities, such as O_2, during the ablation, and use of well maintained ablation systems that are fully flushed and sealed against the atmosphere, as well as the importance of close matrix-matching between standards and unknown samples. Since the goal of the geoanalytical community is to reduce the present-day 2% interlaboratory bias[56] of U–Pb zircon dating by laser ablation ICP-MS to, or below, 1%, it is important that monitoring the oxygen level and maintaining a constant value during an analysis session becomes part of the laboratory routine.

The benefits of signal enhancement from the addition of O_2 to the He sample carrier gas remain to be fully evaluated, and require long-term datasets obtained by analysis of a variety of zircon compositions using a range of LA ICP-MS instruments and operating conditions. The present study shows, however, that maintaining a constant level of O_2 throughout the ablation cell and over an analytical session is a prerequisite for further improvement in U–Pb age repeatability.

Acknowledgements

This study benefited from discussions with Henry Longerich while on a research visit to the Geological Survey of Canada.

Published on 18 February 2014. Downloaded by GFZ POTSDAM WISSENSCHAFTSPARK on 29/10/2014 10:14:04.

Comments by two anonymous reviewers helped to improve the quality of the manuscript. The authors acknowledge the support received from the Czech Science Foundation (project P210/12/2114) and the GSC.

References

1 R. Feng, N. Machado and J. Ludden, *Geochim. Cosmochim. Acta*, 1993, **57**, 3479–3486.
2 B. J. Fryer, S. E. Jackson and H. P. Longerich, *Chem. Geol.*, 1993, **109**, 1–8.
3 T. Hirata and R. W. Nesbitt, *Geochim. Cosmochim. Acta*, 1995, **59**, 2491–2500.
4 S. E. Jackson, H. P. Longerich, I. Horn and G. R. Dunning, *J. Conf. Abs.*, 1996, **1**, 283.
5 J. M. Hanchar and P. W. O. Hoskin, *Zircon. Rev. Mineral. Geochem.*, 2003, vol. 53, p. 500.
6 H. R. Kuhn and D. Günther, *Anal. Chem.*, 2003, **75**, 747–753.
7 M. Guilong and D. Günther, *J. Anal. At. Spectrom.*, 2002, **17**, 831–837.
8 J. Kosler, M. Wiedenbeck, R. Wirth, J. Hovorka, P. Sylvester and J. Mikova, *J. Anal. At. Spectrom.*, 2005, **20**, 402–409.
9 L. P. Black, *et al.*, *Chem. Geol.*, 2004, **205**, 115–140.
10 C. M. Allen and I. H. Campbell, *Chem. Geol.*, 2012, **332–333**, 157–165.
11 E. Kooijman, J. Berndt and K. Mezger, *Eur. J. Mineral.*, 2012, **24**, 5–21.
12 W. C. Butterman and W. R. Foster, *Am. Mineral.*, 1967, **52**, 880–885.
13 K. M. Ansdell and T. K. Kyser, *Am. Mineral.*, 1993, **78**, 36–41.
14 H. J. Chapman and J. C. Roddick, *Earth Planet. Sci. Lett.*, 1994, **121**, 601–611.
15 L. M. Heaman and A. N. LeCheminant, *Chem. Geol.*, 1993, **110**, 95–126.
16 J. Kosler, *Mineral. Assoc. Can., Short Course Ser. MAC Short Course Ser.*, 2012, **42**, 185–202.
17 S. M. Eggins, L. P. J. Kinsley and J. M. G. Shelley, *Appl. Surf. Sci.*, 1998, **129**, 278–286.
18 A. J. G. Mank and P. R. D. Mason, *J. Anal. At. Spectrom.*, 1999, **14**, 1143–1153.
19 R. R. Parrish, *et al.*, *J. Conf. Abs.*, 1999, **4**, 799.
20 J. Košler, *Mineral. Assoc. Can., Short Course Ser. MAC Short Course Ser.*, 2008, **40**, 79–92.
21 J. Koch, M. Wälle, J. Pisonero and D. Günther, *J. Anal. At. Spectrom.*, 2006, **21**, 932–940.
22 I. Horn and F. von Blanckenburg, *Spectrochim. Acta, Part B*, 2007, **62**, 410–422.
23 M. Guillong, I. Horn and D. Günther, *J. Anal. At. Spectrom.*, 2003, **18**, 1224–1230.
24 I. Horn, R. L. Rudnick and W. F. McDonough, *Chem. Geol.*, 2000, **167**, 405–425.
25 J. Košler, H. Fonneland, P. Sylvester, M. Tubrett and R. B. Pedersen, *Chem. Geol.*, 2002, **182**, 605–618.
26 C. Paton, J. D. Woodhead, J. C. Hellstrom, J. M. Hergt, A. Greig and R. Maas, *Geochem., Geophys., Geosyst.*, 2010, **11**, Q0AA06.
27 C. Paton, J. C. Hellstrom, P. B. Bence, J. D. Woodhead and J. M. Hergt, *J. Anal. At. Spectrom.*, 2011, **26**, 2508–2518.
28 S. E. Jackson, *Geochim. Cosmochim. Acta*, 2009, **73**, A579.
29 B. K. Kuhn, K. Birmaum, Y. Luo and D. Günther, *J. Anal. At. Spectrom.*, 2010, **25**, 21–27.
30 I. Horn, M. Guillong and D. Günther, *Appl. Surf. Sci.*, 2001, **182**, 91–102.
31 D. Günther and C. A. Heinrich, *J. Anal. At. Spectrom.*, 1999, **14**, 1369–1374.
32 C. M. Petibon, H. P. Longerich, I. Horn and M. N. Tubrett, *Appl. Spectrosc.*, 2002, **56**, 658–664.
33 T. Hirata, *Anal. Chem.*, 2003, **75**, 228–233.
34 J. Kosler, H. P. Longerich and M. N. Tubrett, *Anal. Bioanal. Chem.*, 2002, **374**, 251–254.
35 K. Nishiguchi, K. Utani and E. Fujimori, *J. Anal. At. Spectrom.*, 2008, **23**, 1125–1129.
36 R. Kovacs, K. Nishiguchi, K. Utani and D. Günther, *J. Anal. At. Spectrom.*, 2010, **25**, 142–147.
37 S. F. Durrant, *Fresenius' J. Anal. Chem.*, 1993, **347**, 389–392.
38 N. N. Sesi, A. MacKenzie, K. E. Shanks, P. Yang and G. M. Hieftjie, *Spectrochim. Acta, Part B*, 1994, **49**, 1259–1282.
39 S. M. Burchell, *Investigations of mixed-gas plasmas using a sheathing device for ICP-MS*, MSc thesis Queen's University Kingston, 2000, p. 161.
40 M. Guillong and C. A. Heinrich, *J. Anal. At. Spectrom.*, 2007, **22**, 1488–1494.
41 S. F. Durrant, *Fresenius' J. Anal. Chem.*, 1994, **349**, 768–771.
42 S. Greenfield, I. L. Jones, H. McGreachin and P. B. Smith, *Anal. Chim. Acta*, 1975, **74**, 225–245.
43 Z. Hu, S. Gao, Y. Liu, S. Hu, H. Chen and H. Yuan, *J. Anal. At. Spectrom.*, 2008, **23**, 1093–1101.
44 R. C. Hutton, *J. Anal. At. Spectrom.*, 1986, **1**, 259–263.
45 M. J. van de Sande, P. van Eck, A. Sola, A. Gamero and J. J. A. M. van der Mullen, *Spectrochim. Acta, Part B*, 2003, **58**, 457–467.
46 S. E. Jackson, N. J. Pearson, W. L. Griffin and E. A. Belousova, *Chem. Geol.*, 2004, **211**, 47–69.
47 L. P. Black and B. L. Gulson, *BMR J. Aust. Geol. Geophys.*, 1978, **3**, 227–232.
48 P. J. Sylvester and M. Ghaderi, *Chem. Geol.*, 1997, **141**, 49–65.
49 R. Wirth, *Eur. J. Mineral.*, 2004, **16**, 863–876.
50 R. Wirth, *Chem. Geol.*, 2009, **261**, 217–229.
51 A. H. Wang, W. Y. Wang, C. S. Xie, W. L. Song and D. W. Zeng, *Appl. Surf. Sci.*, 2004, **227**, 104–113.
52 C. E. Curtis and H. G. Sowman, *J. Am. Chem. Soc.*, 1953, **36**, 190–198.
53 S. Ellsworth, A. Navrotsky and R. C. Ewing, *Phys. Chem. Miner.*, 1994, **21**, 140–149.
54 I. Farnan and E. K. H. Salje, *J. Appl. Phys.*, 2001, **89**, 2084–2090.
55 M. Cai, D. A. Haydar, A. Montaser and J. Mostaghimi, *Spectrochim. Acta, Part B*, 1997, **52**, 369–386.
56 J. Kosler, *et al.*, *Geostand. Geoanal. Res.*, 2013, **37**, 243–259.

 This journal is © The Royal Society of Chemistry 2014